Research Paper

GEOSPHERE

GEOSPHERE; v. 12, no. 2

doi:10.1130/GES01175.1

13 figures; 3 tables

CORRESPONDENCE: dhuo@stanford.edu

CITATION: Huo, D., Pini, R., and Benson, S.M., 2016, A calibration-free approach for measuring fracture aperture distributions using X-ray computed tomography: Geosphere, v. 12, no. 2, p. 558–571, doi:10.1130/GES01175.1.

Received 10 February 2015
Revision received 7 November 2015
Accepted 14 January 2016
Published online 5 February 2016

A calibration-free approach for measuring fracture aperture distributions using X-ray computed tomography

Da Huo[1], Ronny Pini[2], and Sally M. Benson[1]

[1]Department of Energy Resources Engineering, Stanford University, Green Building, Room 065, 367 Panama Street, Stanford, California 94305, USA
[2]Petroleum Engineering Department, Colorado School of Mines, Marquez Hall #206, 1600 Arapahoe Street, Golden, Colorado 80401, USA

ABSTRACT

Various methods have been proposed to measure fracture aperture distributions, including X-ray computed tomography (CT) imaging, which has the advantage that it can be combined with dynamic flow experiments. In this paper, we present a calibration-free missing CT attenuation (CFMA) imaging method for measuring fracture apertures that avoids time-consuming calibration. In addition, this model does not assume a homogeneous matrix and thus provides a good estimate of fracture apertures even when rock properties are heterogeneous. The validity of the CFMA model is established by four approaches: comparing apertures calculated with the conventional calibration-based method; evaluating model predictability at different scanner voxel sizes; comparing with calibration coefficients in the literature from a number of experiments with different rocks and X-ray scanners; and comparing aperture measurements for dry and wet scans. We analyze the systematic error and the random error introduced by rock heterogeneities and CT scanning and show that by averaging 5 replicate scans, we reduce the aperture measurement error to ~22 μm.

INTRODUCTION

Efforts to quantify fracture geometry and tortuosity and their relationship to fracture permeability have been ongoing for decades. Of particular interest are the mechanical opening of fractures, or the aperture, and their spatial distribution. Various methods have been proposed and implemented to measure fracture apertures and to characterize fracture void geometry. Representative techniques (Committee on Fracture Characterization and Fluid Flow et al., 1996) include (1) those that use measurements of surface profilometry; (2) those that involve material filling in the void space; and (3) those that apply noninfiltrative technology, such as computed tomography (CT) scanning.

Table 1 lists 10 methods for measuring fracture apertures (Glover et al., 1998; Isakov et al., 2001; Boutt et al., 2006; Bandis, 1980; Committee on Fracture Characterization and Fluid Flow et al., 1996; Gale, 1987; Billaux and Gentier, 1990; Pyrak-Nolte et al., 1987; Schrauf and Evans, 1986; Barton et al., 1985; Ketcham et al., 2010). The advantages and disadvantages of the methods are also listed. As Table 1 shows, the CT scanning technique alone has the advantage that it can be combined with core-flooding experiments to measure properties such as relative permeability and capillary pressure, stress-dependent transport properties, or reactive chemical transport phenomena, and it is therefore the focus of this paper.

Methods for using X-ray CT scanners to measure fracture apertures have been under development since the 1990s (Johns et al., 1993; Ketcham et al., 2010). There are three alternative conceptual approaches for calculating fracture apertures from CT data, denoted as peak height (PH), full-width-half-maximum (FWHM), and missing CT attenuation (CT_{MA}) in Figure 1. The black line shows a hypothetical transect across the two fractures shown in the inset, which is obtained from an X-ray scan of a rock slice. For this example, the rock matrix has an average CT number of 1250 Hounsfield units (HU), and the presence of a fracture is indicated by lower CT numbers. The HU scale is a representation of the material radiodensity. The CT number of distilled water at standard temperature and pressure (STP) is defined as 0 HU, while the CT number of air at STP is defined as –1000 HU (Hounsfield, 1980).

The area shown by the shaded regions in Figure 1 is called CT_{MA}, which refers to the deficit of density (and, accordingly, X-ray attenuation measured in CT numbers) caused by a fracture filled with air or any other fluid. The first method for calculating fracture aperture, shown in Figure 1, uses the so-called FWHM value, i.e., the width of the transect measured at the midpoint CT number between the air and the rock matrix (125 HU in Fig. 1). One of the drawbacks of the FWHM method is that for thinner apertures, the decrease in CT number may not be sufficiently large to reach the midpoint, and FWHM consequently cannot be used to calculate the aperture (Ketcham and Carlson, 2001). The second method (Fig. 1) uses PH, which corresponds to the difference between the CT number of the rock matrix and the minimum CT value measured across the fracture (Vandersteen et al., 2003). The PH method fails when the fracture aperture is large enough for the minimum CT number to reach the attenuation of air, thus becoming insensitive to the width of the aperture. Note that both the FWHM and PH methods need careful calibration to obtain the relationship between fracture apertures and FWHM/PH. The third method, the CT_{MA}, is shown in the shaded area of Figure 1. This method calculates the CT_{MA} due to the presence of the fracture (Johns et al., 1993; Keller, 1997; Van Geet and Swennen, 2001). The method assumes that all X-ray attenuation is conserved in CT scanning and that the aperture of a fracture can be ascertained if its total attenuation signal can be delineated and integrated. It has been shown

TABLE 1. METHODS IN MEASURING MECHANICAL APERTURES OF FRACTURES

Methods	Mechanism	Advantages	Disadvantages	Citations
Mechanical profilometer	Surface profilometry	High resolution	Sample needs to be taken apart	Glover et al. (1998)
Optical methods	Surface profilometry	High resolution	Sample needs to be taken apart	Isakov et al. (2001)
Laser profilometer	Surface profilometry	High resolution	Sample needs to be taken apart	Boutt et al. (2006)
Tapered filler gauge	Material filling	Easy to measure	Cannot obtain local aperture distribution	Bandis (1980)
Polyester film	Material filling	Good estimates of local aperture geometry	Overestimate the contact area; sample needs to be taken apart	Committee on Fracture Characterization and Fluid Flow et al. (1996)
Epoxy	Material filling	Local aperture and void distribution can be obtained	Sample needs to be taken apart and consequently destroyed	Gale (1987); Billaux and Gentier (1990)
Wood's metal	Material filling	Estimates of areal distribution of void space	Difficult to obtain local aperture geometry	Pyrak-Nolte et al. (1987)
Gas volume measurement	Material filling	Easy to set up instruments	Cannot obtain aperture distribution	Schrauf and Evans (1986)
Borehole pumping tests	Material filling	Easy method in large fractures	Equals mechanical aperture with hydraulic aperture	Barton et al. (1985)
Computed Tomography scanning	Noninfiltrative	In-situ measurement and can be combined with flow experiments	Resolution problems	Ketcham et al. (2010)

that by capturing the density deficit caused by the presence of a fracture, the CT_{MA} method provides for the most accurate estimates of fracture apertures over a wide range of values (Ketcham et al., 2010).

The CT_{MA} is defined by Equation 1 (Ketcham et al., 2010):

$$CT_{MA} = \sum_{i=1}^{N_{vox}} (CT_{mat} - CT_i), \quad (1)$$

where CT_{mat} represents an arbitrary baseline CT value (usually, the average CT number of the rock matrix), CT_i represents the CT values of the transect across the trough, and N_{vox} represents the number of voxels within the trough. Because CT numbers are discrete, we use the summation in all calculations. The relationship between the CT_{MA} and the fracture aperture is determined using careful calibration with spacers of known thickness. Summation of the missing CT values across the trough has a linear relationship with the fracture aperture (Johns et al., 1993):

$$CT_{MA} = d \cdot \text{constant}, \quad (2)$$

where d represents the fracture aperture, and the constant depends on the rock properties and CT scanner specifications.

Although the conventional CT method can be used to measure fracture apertures, it has several shortcomings in the way that it is conventionally applied: first, it requires a significant effort for calibration, normally two to three days for four calibration points using spacers of different thicknesses; second, it typically assumes a homogeneous core, as indicated by the constant in Equation 2. As an alternative to calibration using spacers, Ketcham et al. (2010) demonstrated that apertures could be calculated using an absolute scale, which only requires measuring the CT numbers for the rock matrix and air; however, they concluded that it was difficult to determine the CT value for air inside the core holder due to factors such as beam hardening and image reconstruction artifacts when there are large contrasts between materials.

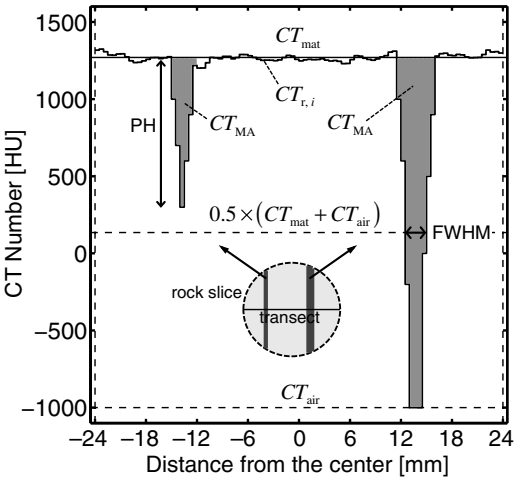

Figure 1. Computed tomography (CT) transect of two hypothetical fractures imaged with an X-ray CT scanner on a slice of a rock sample. The gray-shaded regions represent the so-called missing attenuation (CT_{MA}), while PH and FWHM refer to peak height and full width at half maximum, respectively (see text). HU—Hounsfield units. Scanner resolution is 500 μm (modified after Ketcham et al., 2010).

Ketcham et al. (2010) proposed an enhancement of the CT method that uses a point-spread function (PSF) to relate fracture aperture and variation of the CT numbers across the fracture. By evaluating the shape of the CT traverses over the fracture, accurate measurement of fracture apertures can be obtained

through the inverse PSF method (IPSF). IPSF deals very well with heterogeneity, even for highly heterogeneous materials. With IPSF, apertures of one-tenth of a voxel width can be detected and determined. In general, IPSF provides a robust way to calculate aperture distributions; however, it requires complex numerical deconvolution and is thus more computationally expensive. In addition, the IPSF method does not eliminate the need for a calibration process.

The objective of this paper is to present a more efficient method based on the missing attenuation (MA) approach for calculating fracture aperture distributions that does not require calibration and can be used in heterogeneous rocks with error quantification. The method, referred to here as the CFMA (calibration-free missing attenuation) method, builds on and extends the absolute calibration method described in Ketcham et al. (2010).

SIMPLIFIED METHOD FOR APERTURE MEASUREMENT USING CT SCANNING

The CT number in the vicinity of the fracture is reduced due to the density deficit of the fluid-filled or air-filled fracture. Low CT numbers occur both in the voxels at the fractures and adjacent voxels due to smearing of the X-ray attenuation and so-called partial volume effects (Weerakone and Wong, 2006). The partial volume effect causes the CT number to decrease in the voxels adjacent to the fracture when only a portion of the voxel is filled with rock. Moreover, when material properties change rapidly, smearing of X-ray attenuation occurs due to the finite beam width and oversampling associated with X-ray computed tomography (Johns et al., 1993). These two effects prevent voxels at a density discontinuity from responding sharply to density contrasts. Depending on the rock type and the aperture size, for a scanner with a spatial resolution of 0.5 mm, most of the fractures will affect ~5–6 voxels. Figure 2 illustrates this: three one-dimensional (1-D) transects across a rock slice are shown that represent a hypothetical fracture of width d filled with air (left transect) and the corresponding profile that would be imaged from an X-ray scan (transect in the center) with resolution R. For the sake of simplicity, this illustrative example considers a fracture having a width that corresponds to the resolution of the scanner; note that the process could be repeated for a fracture with an arbitrary width, and the analysis and conclusions that follow would not be affected.

The basic assumption made about using the CT scanning technique is that the total amount of missing attenuation is conserved, even though the influence of the fracture is spread out over a number of voxels (Ketcham et al., 2010). In other words, the gray-shaded regions outlined by the left and center transects have the same area; it follows that the true missing attenuation is defined as

$$\mathrm{CT_{MA}} = \sum_{i=1}^{N_{vox}} (\mathrm{CT_{r,i}} - \mathrm{CT_i}), \tag{3}$$

where $\mathrm{CT_{r,i}}$ are the voxel CT values of the original intact rock matrix, and $\mathrm{CT_i}$ are the corresponding values measured across the trough. The missing attention due to the presence of a fracture can be calculated using the assumption that $\mathrm{CT_{MA}}$ is conserved, which results in the following identity:

$$d \cdot (\mathrm{CT_{r,k}} - \mathrm{CT_{air}}) = R \cdot \mathrm{CT_{MA}}, \tag{4}$$

where $\mathrm{CT_{r,k}}$ is the voxel CT value of the missing matrix along the fracture, and R is the voxel size, or the resolution of the CT scanner. Note that $\mathrm{CT_{r,k}}$ represents the true CT value of the missing matrix along the fracture and is not iterative, while $\mathrm{CT_{r,i}}$ represents a set of iterative CT numbers that are perpendicular to the fracture. Because $\mathrm{CT_{MA}}$ is conserved, Equations 3 and 4 can be equated, resulting in

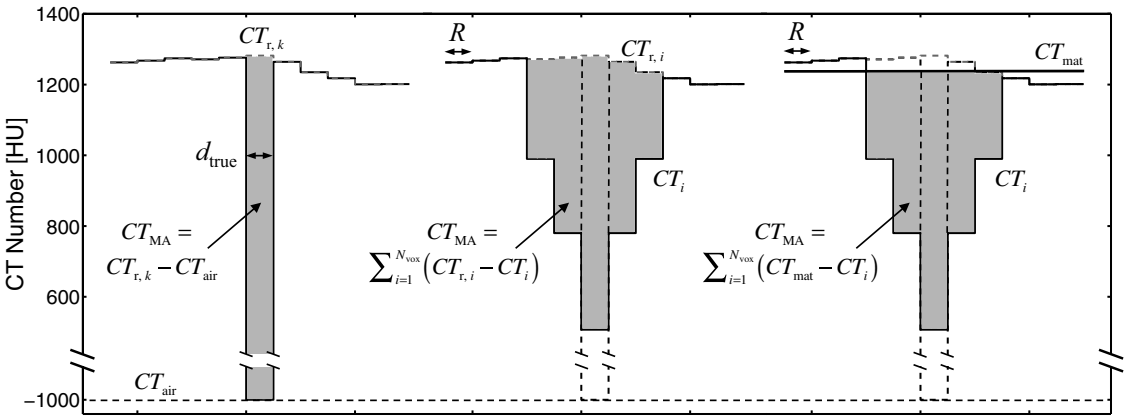

Figure 2. The appearance of a hypothetical fracture on an X-ray computed tomography (CT) scan as represented by one-dimensional transects across a rock slice (see text for abbreviations). HU—Hounsfield units. Left: perfect (ideal) imaging of the fracture, with the transect providing a one-to-one true representation of the original fracture width. Center: imaging of the fracture affected by smearing of X-ray attenuation and scanner resolution. The gray shaded area corresponds to the original missing attenuation. Right: The gray shaded area is obtained by assuming a baseline for the CT number of the intact rock.

$$d = \frac{R \cdot \sum_{i=1}^{N_{vox}} (CT_{r,i} - CT_i)}{CT_{r,k} - CT_{air}}. \quad (5)$$

The main issue in applying Equation 5 is that in a real situation neither $CT_{r,k}$ nor the $CT_{r,i}$ is known. Therefore, in this study a baseline value CT_{mat} is introduced that defines a reference for calculating CT_{MA}:

$$d = \frac{R \cdot \sum_{i=1}^{N_{vox}} (CT_{mat} - CT_i)}{CT_{mat} - CT_{air}}, \quad (6)$$

where CT_{mat} is estimated from the average of six adjacent neighbor voxels just outside the trough region (three on each side of the trough), as depicted in Figure 2 (right-most transect). A value for CT_{air} is also required. For this study we use the value of –1000 HU, as is the convention for making porosity measurements using medical X-ray CT (Akin and Kovscek, 2003). However, as mentioned in Ketcham et al. (2010), beam hardening or other image reconstruction errors will cause CT_{air} to differ from this value inside the core holder. Two approaches for addressing this issue have been proposed: CT_{air} value could be measured directly inside the core holder or calculated from calibration data using spacers of known thickness (Ketcham et al., 2010). Our studies confirm that direct measurements of CT_{air} inside the core holder are not reliable, as indicated by Ketcham et al. (2010). Instead, we calculate the values of CT_{air} from the calibration data for the two rock samples used here. The values of CT_{air} are –1006 HU and –1145 HU. Thus assuming a value of –1000 HU for CT_{air} results in 0.3% and 5% overestimation of the fracture apertures for the 2 samples, with overestimation being larger for the denser rock. Given the benefits of avoiding the need for calibration, approximating CT_{air} = –1000 is acceptable. If denser rocks are used (e.g., ultramafic rocks), beam hardening will be greater and calibration to measure CT_{air} may be required.

For highly heterogeneous materials, the CT numbers might continue increasing from the fracture for more than three voxels. This will cause inaccuracies in the CFMA method; however, examination of the scans can be used to assess whether this is problematic for any particular rock sample. Errors associated with the estimation of CT_{MA} are described herein (see the Discussion). As to the application of the CFMA method, the use of Equation 6 accounts for heterogeneity in the rock properties by using local values for CT_{mat}.

APPLICATION OF THE CFMA METHOD

Materials

Two rock samples were used to test and evaluate the CFMA method; a high-porosity (~22%) Berea Sandstone core (Cleveland Quarries, Vermilion, Ohio, USA) and a low-porosity (< 4%) silicate-cemented sandstone core from southern Israel, which was collected from the Zenifim Formation at a depth of ~1770 m and preserved at the archive of the Geological Survey of Israel. Both samples have a single centered saw-cut fracture that crosses the core through its entire length. The fracture is smoother for the highly cemented Zenifim sandstone as compared to that in the Berea Sandstone, where grains are removed from the surface during sawing. The Berea Sandstone has a length of 8 cm, and the Zenifim sandstone has a length of 6.7 cm; both samples have a diameter of 5 cm.

Imaging Methods

Imaging was carried out as follows: the dried core sample was wrapped in a sleeve with layering from the core outward of one layer of heat-shrinkable Teflon and a Viton rubber sleeve, mounted in an aluminum core holder, and a slight annular pressure (water) of 0.34 MPa was applied to keep the core halves together. The core holder is then placed horizontally in a medical X-ray CT scanner (General Electric HiSpeed CT/i X-ray) that is used to image the fractured samples. The calibration uses spacers made from tin of various widths (~0.20, 0.30, 0.40, 0.50 mm). The spacers are placed between the two rock surfaces, separately at the inlet, the center, and the outlet of the rock sample, and scans are taken at positions between the spacers (for a total of four different slices). For the measurements without spacers, the entire core is imaged. Unless otherwise stated, the following imaging parameters have been applied in this study: voxel dimension of (0.5 × 0.5 × 1) mm^3, a display field of view of 25 cm, a tube current of 200 mA, and an energy level of 120 keV. CT_{MA} due to the presence of the fracture is calculated using Equation 1. Calculating the CT_{MA} due to the presence of a fracture requires data cropping, classification, and identification of fracture features (Karpyn et al., 2009). The location of the fracture is identified with the lowest CT number within the trough, which extends on both sides of the fracture until the point where the CT number stops increasing. The definition of the trough edge might result in an increased matrix CT number estimate, which will increase the calculated CT_{MA} and further raise the fracture aperture measurement. The matrix CT number CT_{mat} is calculated by averaging the CT numbers of six adjacent voxels next to the trough region (three on each side). The fracture aperture is then calculated either with Equation 6 or through the calibration method, as suggested in previous studies. To reduce the random noise that affects X-ray images, multiple scans are taken at identical locations and averaged, following a protocol presented in Pini et al. (2012). For the calibration, 20 repeated scans are taken and averaged to further reduce the CT scanning error.

Fracture Aperture Measurement Using the Conventional Calibration Method

Illustrative snapshots of X-ray scans acquired with different spacers within both fractured samples are shown in Figure 3. Figure 4 shows the corresponding transect lines that pass through a given location of the core for the Berea Sandstone sample. While the number of voxels spanning the trough region remains constant (five voxels in the figure), the CT number in the fracture region drops

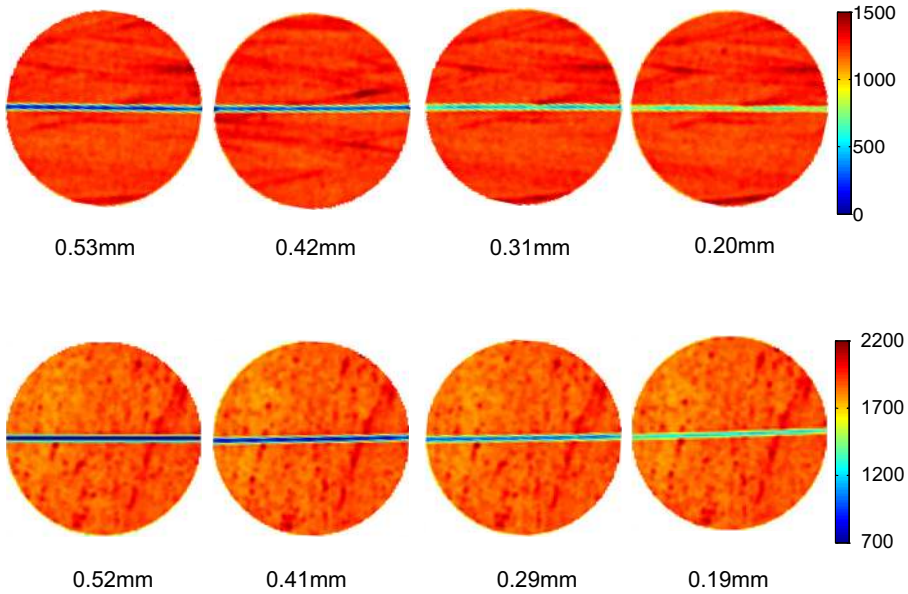

Figure 3. Two-dimensional X-ray images of a fractured sample containing spacers with various thicknesses. Top: Berea Sandstone core. Bottom: Zenifim sandstone core. The color scale indicates computed tomography (CT) numbers. Each image represents the average of 20 repeated scans taken at the same location with resolution (0.5 × 0.5 × 1) mm³.

gradually with larger spacers, and reaches almost 100 HU for the 0.5-mm-thick spacer. The missing attenuation increases accordingly with aperture size.

CT_{MA} values were calculated with Equation 1 at four distinct locations (slices) within the rock sample and with four different spacers (for a total of 380 points/spacer). Because the fracture surface is rough, the calculated CT_{MA} for each spacer is expected to have a wide distribution (broader for the Berea Sandstone than for the fine-grained Zenifim sandstone sample). The histogram distribution of CT_{MA} values for the 0.53-mm-thick spacer is shown in Figure 5 (inset on left). The CT_{MA} of the fracture is normally distributed; accordingly, vertical bars are added to each symbol in Figure 5 to represent the spread of the distribution. As expected from those methods that use a calibration to define the relationship between CT_{MA} and fracture aperture, CT_{MA} is linearly proportional to spacer thickness. Because the fracture surface is not perfectly smooth, the regression line does not pass through the origin, suggesting that the initial aperture caused by the roughness of the fracture surface is 0.14 ± 0.01 mm and 0.08 ± 0.01 mm for the Berea and Zenifim samples, respectively. Uncertainties of both the slope (M) and the intercept are calculated (Taylor, 1997). In order to build the calibration curve used in calibration methods to estimate fracture aperture, the regression line is shifted to cross the origin of the axes; for the Berea and Zenifim samples, the slopes of these lines are 4512 and 5890 (HU/mm), respectively. According to Equation 6, the slope of the calibration lines should be equal to $\frac{CT_{mat} - CT_{air}}{R}$, when the average rock matrix CT number

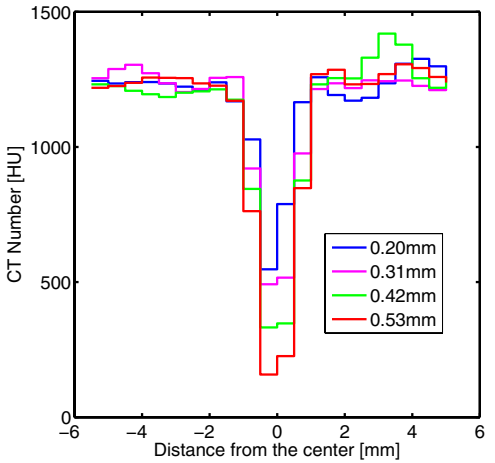

Figure 4. Transect lines drawn at a given location that cross fractures obtained with different spacers for the Berea Sandstone sample. The inset shows the details of the trough region. To draw the transect lines, images have been used that have been obtained from the average of 20 repeated scans taken at the same location with resolution (0.5 × 0.5 × 1) mm³. HU—Hounsfield units.

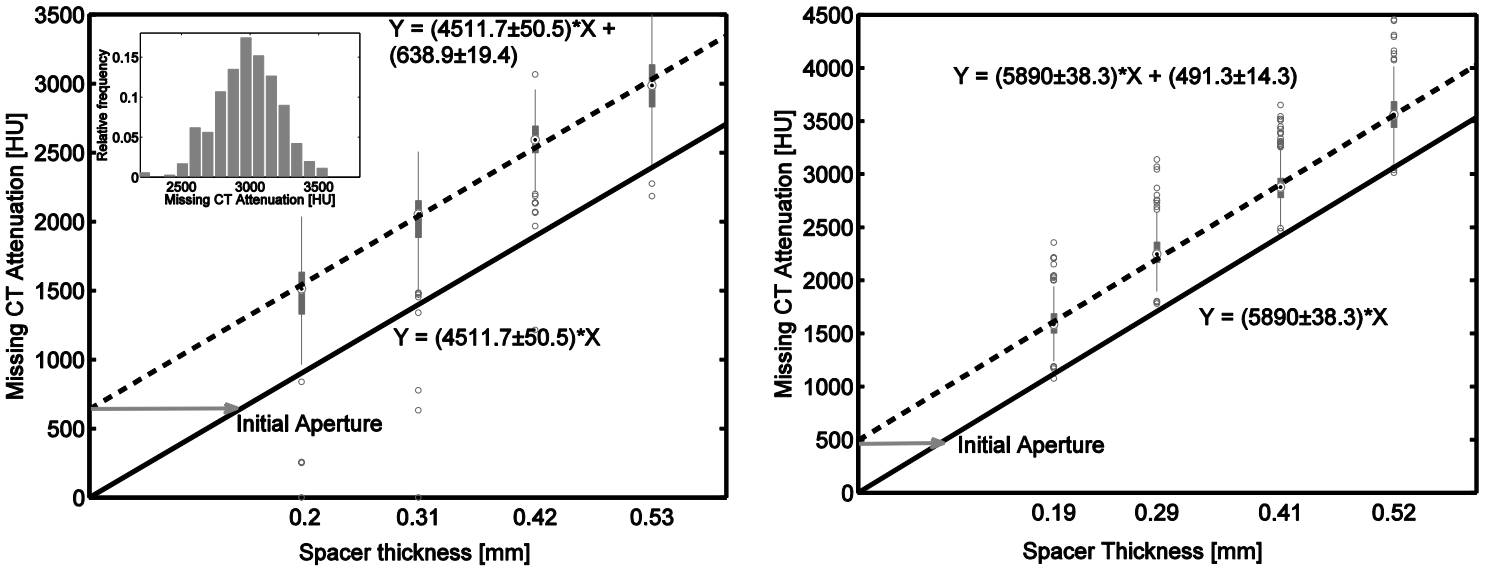

Figure 5. Calibration of fracture apertures for the Berea Sandstone and Zenifim sandstone. The upper left inset shows the distribution of missing attenuation with a spacer thickness of 0.53 mm. The circle with a dot inside shows the median value of all points. The thick gray lines show the 25% confidence interval; the thin gray line shows the 75% confidence interval. The circles above and below the thin gray lines are outliers. The dashed line corresponds to the initial fitting, and the solid line corresponds to the relationship between missing computed tomography (CT) attenuation and fracture aperture. HU—Hounsfield units. The standard deviation for linear fitting is calculated both for the slope and the intercept (Taylor, 1997). A total of 380 points at each spacer thickness are used in the calibration.

is used (1250 HU for Berea Sandstone and 1800 HU for Zenifim sandstone). Accordingly, the slopes for the Berea Sandstone and Zenifim sandstone are expected to be 4500 and 5600 HU/mm, respectively, in agreement within <1% and 5%, respectively, of the slopes calculated from the data.

Note that the use of a calibration line implicitly assumes that the denominator in Equation 5 is a constant, implying that the CT number of the matrix does not vary spatially within the rock. While this may be satisfactory when the average fracture aperture is computed, this assumption has to be relaxed when the goal is to determine aperture distribution of the fracture.

The calibration data can also be used to calculate the value of CT_{air}:

$$CT_{air} = CT_{mat} - M \cdot R, \quad (7)$$

where M is the slope of the calibration curve, R is the scanner resolution, and CT_{mat} is the average CT value for the rock matrix. Using Equation 7, CT_{air} values in the Berea Sandstone and Zenifim sandstone are –1006 and –1145 HU, respectively. The lower value measured in the Zenifim sandstone is consistent with a great degree of beam hardening in the higher density core. We use a constant value of –1000 HU for air in the subsequent calculations, which results in a slight overestimation of the fracture apertures by 0.3% and 5% for the Berea Sandstone and Zenifim sandstone, respectively.

VALIDATION OF THE CFMA METHOD

To evaluate the accuracy and validity of the CFMA method, we apply four tests: linearity between CT_{MA} and resolution of the scanner, as predicted by Equation 6; comparison of the aperture distribution using the conventional calibration-based approach and the CFMA method; comparison between fitting parameters from literature data and predictions using Equation 6; and comparison between aperture distributions made using dry and wet scans.

Linearity Between CT_{MA} and CT Scanner Resolution

To confirm the relationship between CT_{MA} and CT scanner resolution, we conducted a set of experiments under variable fields of view: 10, 15, 20, and 25 cm. The experiments are conducted without spacers, and thus the whole sample is scanned. The corresponding voxel dimensions are (0.2 × 0.2 × 1) mm³, (0.3 × 0.3 × 1) mm³, (0.4 × 0.4 × 1) mm³, and (0.5 × 0.5 × 1) mm³. The computed CT_{MA} is plotted in Figure 6 as a function of the reciprocal of CT scanner resolution, and a linear relationship is found. The dashed line in Figure 6 is the prediction using Equation 6 based on the average matrix CT number (1250 HU for Berea Sandstone and 1800 HU for Zenifim sandstone) and the average frac-

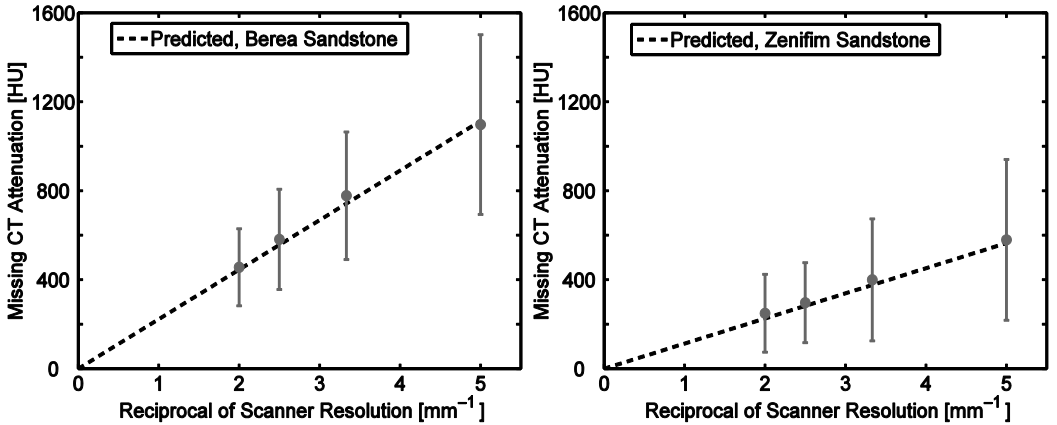

Figure 6. Prediction of missing computed tomography (CT) attenuation at different CT scanner resolutions. HU—Hounsfield units. The solid circle shows the median value of all aperture values of the fracture. The gray bars show one standard deviation of the aperture values at different scanner resolutions. The dashed line shows the prediction of missing CT attenuation using Equation 6 (CT_{MA}; see text).

ture aperture (0.099 mm for Berea Sandstone and 0.040 mm for Zenifim sandstone); as shown in Figure 6, it agrees well with the CT_{MA} at different CT scanner resolutions.

Comparison between the Calibration Method and the CFMA Method

We compare apertures calculated with the conventional calibration-based method and the CFMA method. Table 2 shows the differences between fracture apertures for both rocks obtained by using Equation 6 and those obtained from the calibration lines shown in Figure 5. Results are reported in terms of mean apertures and standard deviations, using data generated with spacers spanning 0.2–0.5 mm. In this comparison, the calibration-based method uses a single calibration curve for the whole core, and thus assumes that the core is homogeneous. In contrast, the CFMA method does not require the rock to be homogeneous; instead, it uses local values for CT_{mat} in Equation 6. The mean values and standard deviations of the calculated apertures obtained from the two methods agree very well, with a 1% and 3% difference for mean apertures of the Berea Sandstone and Zenifim sandstone, respectively. The standard deviation differences are slightly larger for the CFMA method ranging from 2% to 9% for the Berea Sandstone and Zenifim sandstone, respectively. Larger differences between the two methods are expected for less homogeneous rocks, because the CFMA method explicitly accounts for the influence of heterogeneity.

As a second test, shown in Figures 7 and 8, we compare aperture distributions calculated using the calibration method and the CFMA method when no spacer is present. Both the Berea Sandstone and the Zenifim sandstone are compared. The 2-D fracture images, aperture distributions, and voxel-by-voxel comparisons show that the agreement between the two methods is excellent. The agreement between the aperture distributions calculated using the CFMA method and the traditional calibration-based approach provides further confirmation that the errors associated with assuming CT_{air} is –1000 are negligible.

Comparison between Literature Data and CFMA Model Prediction

Results of nine experiments from different authors are examined to evaluate the validity of the CFMA method (Keller, 1997; Bertels et al., 2001; Johns et al., 1993; Weerakone and Wong, 2006; Muralidharan et al., 2004; He, 1998).

TABLE 2. COMPARISON OF FRACTURE APERTURES USING THE STANDARD CALIBRATION-BASED METHOD AND THE CFMA METHOD

	Calibration method		CFMA method	
Berea Sandstone spacer (mm)	Mean (mm)	Standard deviation (mm)	Mean (mm)	Standard deviation (mm)
0.5	0.638	0.041	0.645	0.041
0.4	0.577	0.045	0.579	0.045
0.3	0.429	0.053	0.433	0.054
0.2	0.310	0.057	0.313	0.058
Zenifim sandstone spacer (mm)				
0.5	0.580	0.019	0.596	0.019
0.4	0.463	0.022	0.475	0.024
0.3	0.357	0.024	0.367	0.026
0.2	0.245	0.022	0.252	0.024

Note: CFMA—calibration-free missing computed tomography attenuation. See text Equations 2 and 6.

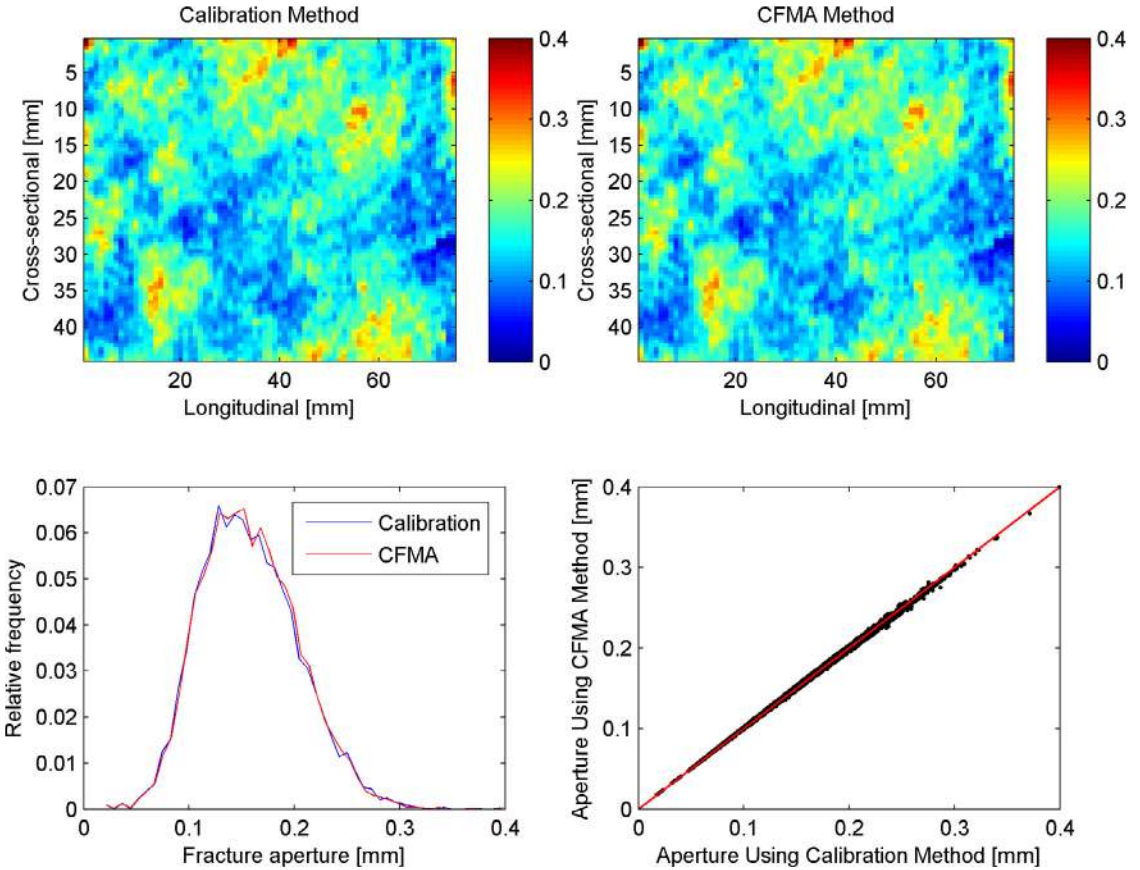

Figure 7. Comparison between the calibration method and the calibration-free missing CT attenuation (CFMA) method for the Berea Sandstone. Upper left: fracture aperture map using the calibration method, where longitudinal direction represents the direction along the core, and cross-sectional direction represents the direction along the diameter of the core. Upper right: fracture aperture map using the CFMA method. Lower left: the relative frequency of fracture aperture distribution for the calibration method and the CFMA method. Lower right: aperture comparison between the calibration method and the CFMA method.

Comparison between the reported calibration coefficients and the values predicted using Equation 6 (using published values for CT_{mat} and the CT scanner resolution) are shown in Figure 9 and Table 3. Agreement is very good, and outliers are only found in Weerakone and Wong (2006) and He (1998). The mismatch might be caused by insufficient information on calculating the MA baseline.

Fracture Aperture Measurements Using Dry and Wet Scans

We further compare the aperture fields measured with water-filled and air-filled fractures. For the water-filled fracture, CT_{wat} (equal to 0 HU) is used instead of CT_{air} in Equation 6. Figure 10 shows the experimental data from the fractured Berea Sandstone. The average aperture for the dry scan is 0.112 mm and the average aperture for the wet scan is 0.113 mm. The difference between the two measurements is provided in Figure 10, which also shows that the distribution of the aperture differences exhibits a normal distribution with mean of –0.0007 mm and standard deviation of 0.043 mm. Good agreement between the values shows that the CFMA method can also be applied to water-filled fractures and provides additional confirmation that using a value of CT_{air} of –1000 HU is satisfactory when using a medical scanner for making fracture aperture measurements.

DISCUSSION

Here we analyze the error related with the CFMA method in two parts: the systematic error (σ_{sys}) and the random error (σ_{rand}). The systematic error originates from the assumption that the CT_{mat} used in Equation 6 can be cal-

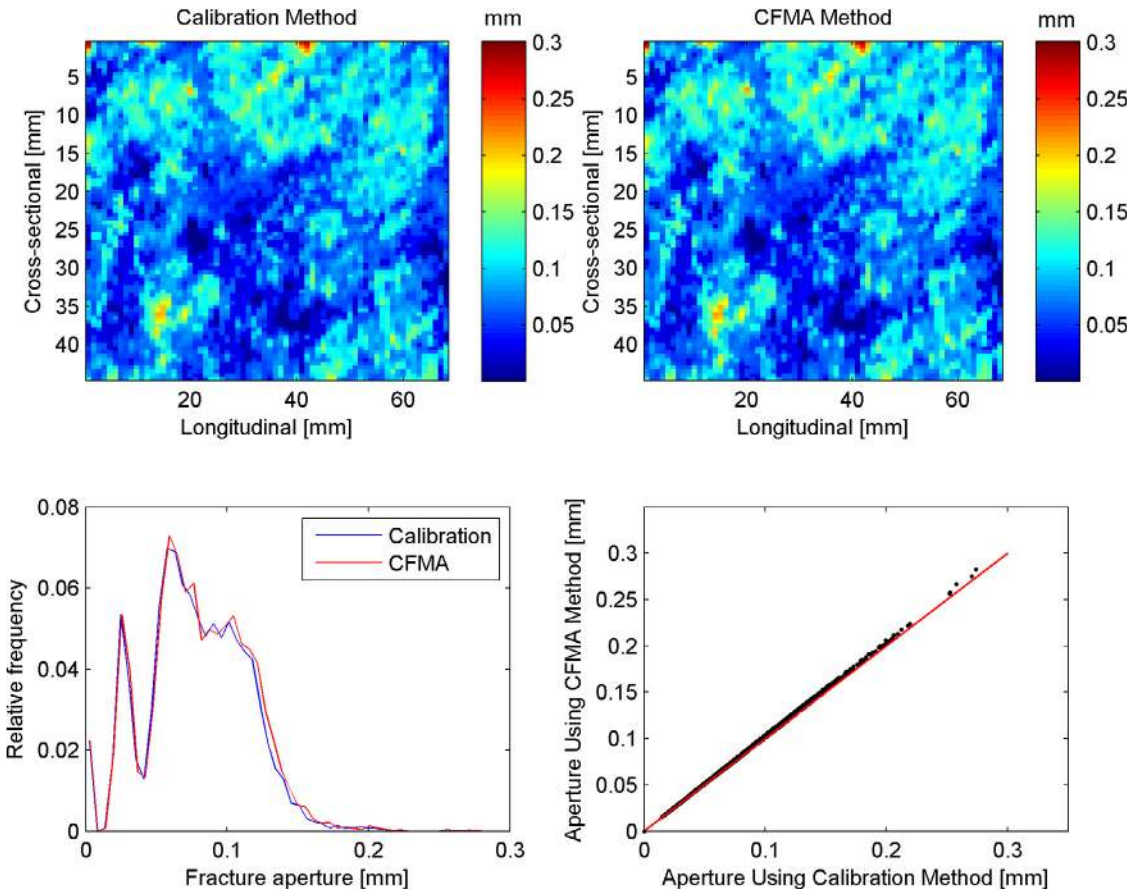

Figure 8. Comparison between the calibration method and the calibration-free missing CT attenuation (CFMA) method for the Zenifim sandstone. Upper left: fracture aperture map using the calibration method. Upper right: fracture aperture map using the CFMA method. Lower left: the relative frequency of fracture aperture distribution for the calibration method and the CFMA method. Lower right: aperture comparison between the calibration method and the CFMA method.

culated from the average of the three voxels on each side of the fracture (six voxels in total). The random error is due to the uncertainties related with CT scanning technique (Pini et al., 2012), which can be reduced by averaging data from replicate measurements. In general, the variance of $c = f(a,b)$ can be estimated:

$$\sigma_c^2 = \sigma_a^2\left(\frac{\partial c}{\partial a}\right)^2 + \sigma_b^2\left(\frac{\partial c}{\partial b}\right)^2 + 2\sigma_{ab}\left(\frac{\partial c}{\partial a}\right)\left(\frac{\partial c}{\partial b}\right), \quad (8)$$

where σ_{ab} represents the covariance between a and b, which can be neglected if a and b are uncorrelated. Here we assume the systematic error and random error are not correlated. The total error (σ_{tot}) is calculated by:

$$\sigma_{tot} = \sqrt{\sigma_{sys}^2 + \sigma_{rand}^2}. \quad (9)$$

As described in the following, combining the systematic error and random error, the total measurement error is ~22 μm with 5 scans using a resolution of 500 μm, which is less than one-twentieth of the voxel size.

Systematic Error

The unavoidable use of a baseline CT value to represent the intact rock matrix (CT_{mat}) in the calculation of CT_{MA} introduces a source of error. In this study, this error has been independently quantified by comparing fracture apertures calculated using Equation 5, which provides the true value for the aperture, and Equation 6, which provides the value based on assuming that CT_{mat} can be approximated by the three adjacent voxels on either side of the fracture. To provide a rigorous test of the systematic error, calculations are made by

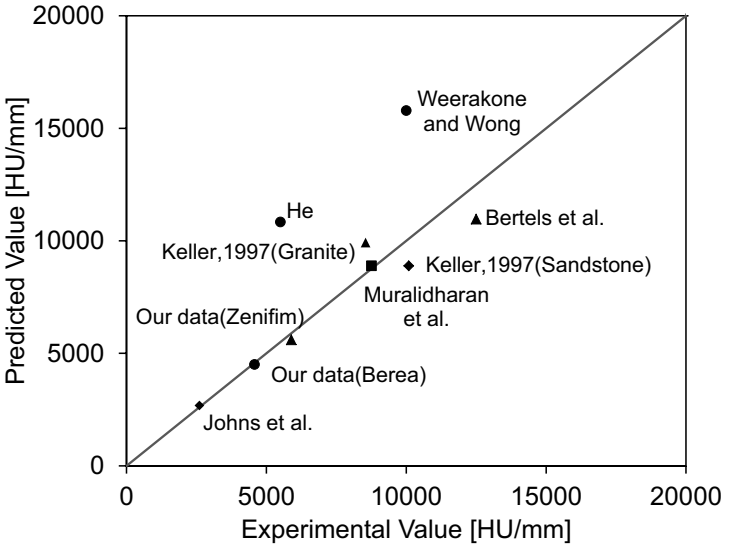

Figure 9. Comparison between predicted values using Equation 6 and values reported in the literature (Bertels et al., 2001; He, 1998; Johns et al., 1993; Keller, 1997; Muralidharan et al., 2004; Weerakone and Wong, 2006). HU—Hounsfield units.

introducing virtual fractures of 100 and 500 μm into the scans. Smearing associated with image reconstruction and other scanning artifacts is added to the 5 voxels adjacent to the fracture such that the CT_{MA} equals that expected for 100 or 500 μm apertures. Figure 11 summarizes this analysis by showing histogram plots of the deviation between true (Equation 5) and computed (Equation 6) apertures for the 100 and 500 μm fracture for scans with an image resolution of 500 μm. In each case, 1650 independent realizations have been performed by placing the given fracture at arbitrary positions within rock slices of a Berea Sandstone core. In both cases, the observations are normally distributed around the true fracture apertures (mean $d - d_{true}$ = 0.5 μm for the 100 μm fracture and $d - d_{true}$ = 0.3 μm for the 500 μm fracture) with standard deviations of ~21 μm. The error introduced by assuming a local baseline CT value for the rock matrix will affect the experimentally estimated fracture aperture with an uncertainty of 21 μm. It is interesting that the repetition of this calculation by imposing the baseline as being the average CT number of the entire slice leads to results that are normally distributed (with similar standard deviations of ~21 μm), but with their mean significantly shifted from zero, i.e., with values of $d - d_{true}$ = 6 μm for 100 μm fracture and 5 μm for 500 μm fracture. We conclude that when compared to calibration methods that assume a transect-, a slice- or a core-averaged value for CT_{mat}, the use in this study of a local value allows us to better capture the inherent spatial heterogeneity of the rock's matrix, while it reduces the systematic error introduced by imposing an arbitrary baseline.

Random Error

For a rock with a uniform composition, the most significant limit of using CT scanning for fracture aperture analysis is the system noise, which will cause errors in aperture estimation. However, repeated scans will help to reduce the error (Pini et al., 2012). Here we analyze the effect of random errors on fracture aperture measurements. Based on Equation 8,

$$\sigma_{vox,n} = \sigma_{vox}/\sqrt{n}, \quad (10)$$

where $\sigma_{vox,n}$ represents the standard deviation of the mean voxel CT value, and σ_{vox} represents the standard deviation associated with a voxel. For the fracture transect illustrated in Figure 12, if we assume that *m* voxels are involved in the

TABLE 3. COMPARISON BETWEEN PREDICTED VALUES USING TEXT EQUATION 6 AND VALUES REPORTED IN LITERATURE

Reference	Rock type	Average matrix CT (HU)	Air CT (HU)	Resolution (mm)	Experimental value (HU/mm)	Prediction (HU/mm)	Difference
Keller (1997)	granite	1680	–1000	0.27	8547	9926	0.16
Keller (1997)*	sandstone	1400	–1000	0.27	10091	8889	0.12
Bertels et al. (2001)	basalt	2400	–1000	0.31	12500	10968	0.12
Johns et al. (1993)*	granite	1680	–1000	0.73	2608	2680	0.03
Weerakone and Wong (2006, personal commun.)	sandstone	2000	–1000	0.19	10000	15789	0.58
Muralidharan et al. (2004)*	sandstone	1400	–1000	0.27	8762	8889	0.01
He (1998)	basalt	2250	–1000	0.30	5503	10833	0.97
Our data (Berea Sandstone†)	sandstone	1250	–1000	0.50	4512	4500	0.00
Our data (Zenifim sandstone†)	sandstone	1800	–1000	0.50	5890	5600	0.05

Note: CT—computed tomography. HU—Hounsfield unit. See text for references.
*Estimated from related rock data.
†Measured by experiment.

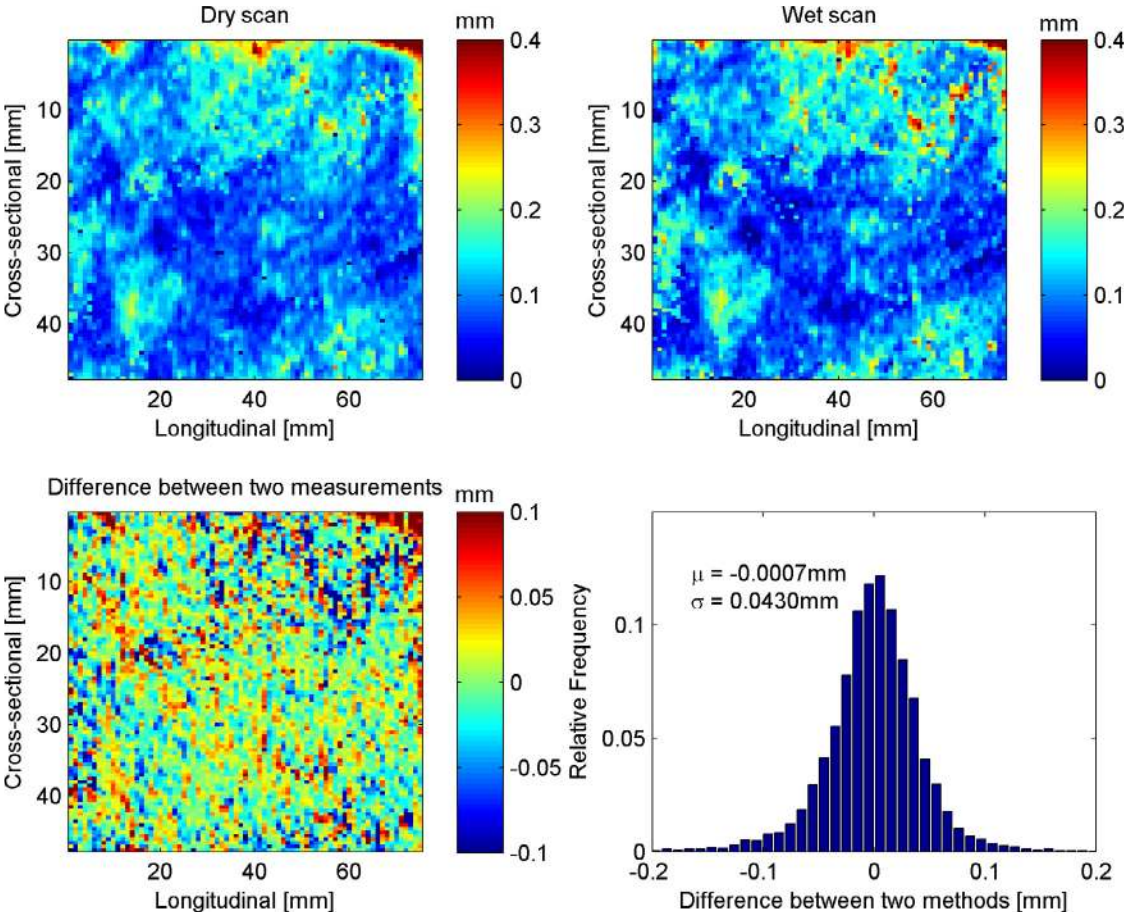

Figure 10. Comparison of fracture aperture distributions using the dry scan and the wet scan for the Berea Sandstone. Upper left: fracture aperture map using the dry scan. Upper right: fracture aperture map using the wet scan. Lower left: the difference between fracture aperture distributions using the dry scan and the wet scan. Lower right: the relative frequency of the difference between fracture aperture distributions for the dry scan and the wet scan. Both the dry scan and the wet scan are averaged from 5 scans.

calculation, according to Equation 8, the standard deviation of CT_{MA} can be calculated from:

$$\sigma^2_{CT_{MA}} = m\sigma^2_{vox,n}. \quad (11)$$

By substituting Equation 10 into Equation 11, we have

$$\sigma_{CT_{MA}} = \sqrt{\frac{m}{n}}\sigma_{vox}, \quad (12)$$

where m is the number of voxels used in the calculation of CT_{MA}, and n is the number of scans. Because of the limited number of data points available to estimate the true sample variance, sample variance theory (Wolter, 2003) is applied to estimate the variance of CT_{MA} as

$$\sigma_{CT_{MA}} = \sqrt{\frac{m}{n-1}}\sigma_{vox}. \quad (13)$$

An example for one representative transect crossing the fracture with a 0.5 mm spacer is shown in Figure 12. The average matrix CT number is calculated using the average of a_1, a_2, a_3 and a_{10}, a_{11}, a_{12}. By subtracting the voxels in the trough (a_4, a_5, a_6, a_7, a_8, a_9) from the baseline, the CT_{MA} will be calculated. In this case,

$$CT_{MA} = 6\times\frac{1}{6}(a_1+a_2+a_3+a_{10}+a_{11}+a_{12}) - a_4 - a_5 - a_6 - a_7 - a_8 - a_9 = a_1+a_2+a_3+a_{10}+a_{11}+a_{12} - a_4 - a_5 - a_6 - a_7 - a_8 - a_9. \quad (14)$$

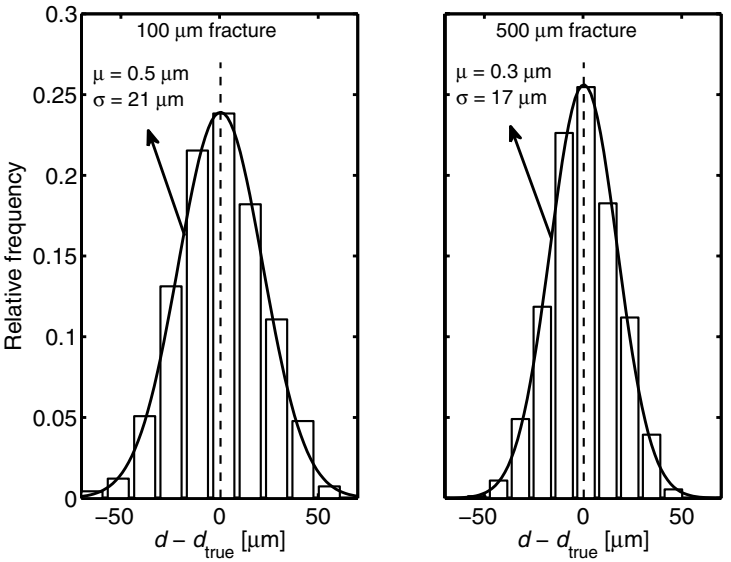

Figure 11. Histogram plot of the deviation between true (d_{true}) and computed (d) fracture aperture, where the later assumes a locally constant matrix computed tomography (CT) number (see text). Two fracture apertures are considered (100 and 500 μm) within rock slices obtained upon averaging 20 repeated scans. Each histogram represents 1650 independent realizations, and normal distribution curves are shown that are predicted from the calculated mean and standard deviation.

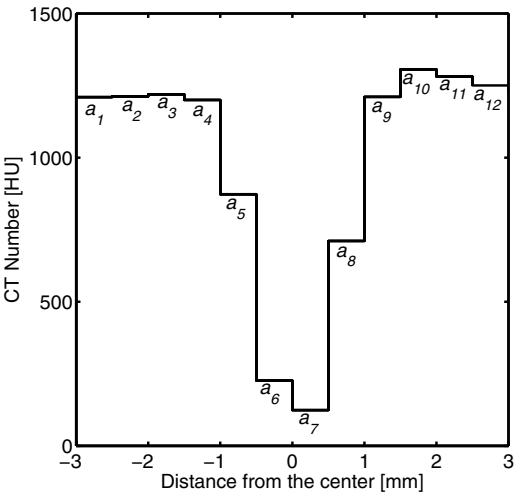

Figure 12. Scan across a fracture showing the voxels for missing attenuation calculation. The trough region includes a_4, a_5, a_6, a_7, a_8, a_9. The average matrix computed tomography (CT) number is calculated by taking average of a_1, a_2, a_3, a_{10}, a_{11}, a_{12} (see text). HU—Hounsfield units.

The standard deviations for each of the voxels in the transect are calculated from 20 replicate scans and are shown in Figure 13. The average value of the standard deviation is 17.66 HU. Because the standard deviations in the matrix area and the trough area have no distinct differences, we use the average value of the standard deviation to calculate CT_{MA} due to random scanning errors, where n is the number of replicate measurements, as

$$\sigma_{CT_{MA}} = \sqrt{\frac{12}{n-1}}\sigma_{vox}. \quad (15)$$

In the case analyzed here, for 5 scans, $\sigma_{CT_{MA}}$ = 30.58 HU; for 2 scans, $\sigma_{CT_{MA}}$ = 61.18 HU. By considering the relationship between CT_{MA} and fracture aperture, the resolution of the measurements made with multiple scans can be calculated using:

$$\sigma_d^2 = \left(\frac{R}{CT_{mat} - CT_{air}}\right)^2 \sigma_{CT_{MA}}^2 + \left(\frac{CT_{MA} \cdot R}{(CT_{mat} - CT_{air})^2}\right)^2 \sigma_{CT_{mat}}^2. \quad (16)$$

Because $\sigma_{CT_{mat}}$ (17.66 HU) is $<\sigma_{CT_{MA}}$, and $\frac{CT_{MA}}{CT_{mat} - CT_{air}}$ is usually <<1, the standard deviation of aperture measurement can be estimated as

$$\sigma_d \approx \frac{R}{CT_{mat} - CT_{air}}\sigma_{CT_{MA}}. \quad (17)$$

For the rocks tested here, $\sigma_d \approx 7$ μm with 5 scans; if only 2 scans are used, the measurement error is ~13 μm. The size of the random error has been validated using the method described by Pini et al. (2012) and was described in detail in Huo (2015).

The overall uncertainty affecting fracture aperture estimates include contributions from both the random noise affecting X-ray measurements (σ_d = 7 μm) and the assumption on the matrix baseline discussed herein (see Systematic Error) (σ_d = 21 μm). The total error is estimated by summing the squares of these two values, thus resulting in a total uncertainty of ~22 μm when the voxel size is 500 μm. Note that we focus here on horizontal fractures. If the fracture is not horizontal or perpendicular, the associated error of fracture aperture measurement could increase because of the Cartesian geometry of the reconstructed image.

For the conventional calibration method, the error is a combination of both the linear fitting error (Fig. 5) and the error of CT_{MA}. By applying the similar

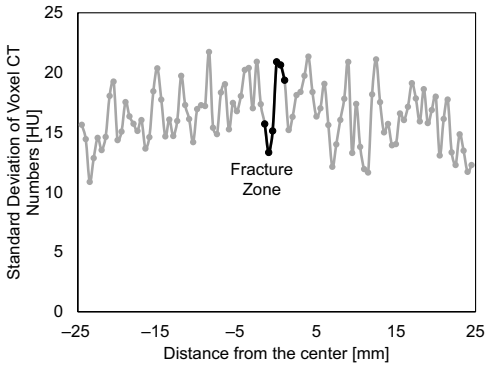

Figure 13. Standard deviation of computed tomography (CT) number across a fracture. HU—Hounsfield units. Black points represent the location of the fracture trough.

error analysis in Equation 16, the standard deviation of aperture measurement is ~28 μm with a single scan, which is very close to the standard deviation of 25 μm from Bertels et al. (2001) using a 310 μm voxel size.

CONCLUSIONS

We have developed a calibration-free missing CT attenuation (CFMA) method for calculating fracture apertures using X-ray CT imaging without time-consuming calibration. Four tests have been applied to test the method's validity based on two rock cores and the literature. The results of these tests suggest that the method provides reliable aperture measurements. Error analysis shows that the method provides a measurement error of 22 μm when 5 replicate scans are averaged, which is less than one-twentieth of the voxel size. Benefits of the CFMA approach include the following.

1. The CFMA method provides a much more convenient and efficient way to relate fracture aperture and CT_{MA}. For a calibration with four spacers, the majority of the time is conventionally spent on core holder mounting and CT scanner machine time. With the CFMA method, the time required for making a set of aperture measurements can be reduced from several days to several hours. Moreover, opening the core holder to adjust the spacers and repositioning it in the field of view introduces additional errors for the measurements.

2. Uncertainty due to random errors is highly reduced by repeated scans, resulting in improved resolution of the fracture apertures. By applying 5 scans, which normally takes 2 h for a core length of 7 cm, the random error can be reduced by 50% compared with a single scan. Repeated scans can also increase the accuracy of matrix CT number, which will reduce the error of the aperture calculation.

3. The method is particularly valuable for combining dynamic core flood experiments with simultaneous aperture measurements, for example, in the study of stress-dependent permeability in fractured rocks (Huo and Benson, 2015). The CFMA method can also be used with water-filled fractures, by substituting CT_{wat} for CT_{air} in Equation 6.

4. This work focuses mainly on sedimentary rocks. The CFMA method may be applicable to other kinds of rocks. The corresponding errors of the method need to be investigated depending on the heterogeneities of the rocks and the extent of beam hardening.

5. The CFMA method demonstrates that the calibration of Hounsfield units embedded in this scanner is sufficient to provide accurate aperture measurements. Other methods, such as IPSF, could potentially use the same approach to eliminate the need for a calibration process. We advise verification of the applicability of the CFMA method for their specific instrument and experiment setups.

ACKNOWLEDGMENTS

This work has been supported by Eni S.p.A. (Rome, Italy). We are grateful to Rani Calvo from the Geological Survey of Israel for providing the Zenifim sandstone sample used in this study.

REFERENCES CITED

Akin, S., and Kovscek, A.R., 2003, Computed tomography in petroleum engineering research, *in* Akin, S., and Kovscek, A.R., eds., Applications of X-ray computed tomography in the geosciences: Geological Society of London Special Publication 215, p. 23–38, doi:10.1144/GSL.SP.2003.215.01.03.

Bandis, S., 1980, Experimental studies of scale effects on shear strength and deformation of rock joints [Ph.D. thesis]: Leeds, West Yorkshire, England, University of Leeds, 540 p.

Barton, N., Bandis, S., and Banktar, K., 1985, Strength, deformation and conductivity coupling of rock joints: International Journal of Rock Mechanics and Mining Sciences & Geomechanics Abstracts, v. 22, no. 3, p. 121–140, doi:10.1016/0148-9062(85)93227-9.

Bertels, S.P., DiCarlo, D.A., and Blunt, M.J., 2001, Measurement of aperture distribution, capillary pressure, relative permeability, and in situ saturation in a rock fracture using computed tomography scanning: Water Resources Research, v. 37, p. 649–662, doi:10.1029/2000WR900316.

Billaux, D., and Gentier, S., 1990, Numerical and laboratory studies of flow in a fracture, *in* Barton, W., and Stephansson, E., eds., Rock joints: Proceedings of the International Symposium on Rock Joints: Rotterdam, A.A. Balkema, p. 369–373.

Boutt, D.F., Grasselli, G., Fredrich, J.T., Cook, B.K., and Williams, J.R., 2006, Trapping zones: The effect of fracture roughness on the directional anisotropy of fluid flow and colloid transport in a single fracture: Geophysical Research Letters, v. 33, L21402, doi:10.1029/2006GL027275.

Committee on Fracture Characterization and Fluid Flow, U.S. National Committee for Rock Mechanics, Geotechnical Board, Board on Energy and Environmental Systems, Commission on Engineering and Technical Systems, and National Research Council, 1996, Rock fractures and fluid flow: Contemporary understanding and applications: Washington, D.C., National Academies Press, 568 p., doi:10.17226/2309.

Gale, J.E., 1987, Comparison of coupled fracture deformation and fluid flow models with direct measurements of fracture pore structure and stress-flow properties, *in* Farmer, I.W., et al., eds., Rock mechanics: Proceedings of the 28th U.S. Symposium on Rock Mechanics: Rotterdam, A.A. Balkema, p. 1213–1222.

Glover, P.W.J., Matsuki, K., Hikima, R., and Hayashi, K., 1998, Fluid flow in synthetic rough fractures and application to the Hachimantai geothermal HDR test site: Journal of Geophysical Research, v. 103, p. 9621–9635, doi:10.1029/97JB01613.

He, M., 1998, Application of X-ray tomography to measurement of fractures in rocks [M.S. thesis]: Stanford, California, Stanford University, 101 p.

Hounsfield, G.N., 1980, Computed medical imaging: Science, v. 210, p. 22–28, doi:10.1126/science.6997993.

Huo, D., 2015, Measuring fracture aperture and water saturation distributions using computed tomography and its application to modeling geomechanical impact on fluid flow in fractures [Ph.D. thesis]: Stanford, California, Stanford University, 185 p.

Huo, D., and Benson, S.M., 2015, An experimental investigation of stress-dependent permeability and permeability hysteresis behavior in rock fractures, *in* Faybishenko, B., et al., eds., Fluid dynamics in complex fractured-porous systems: American Geophysical Union Geophysical Monograph 210, p. 99–114, doi:10.1002/9781118877517.ch7.

Isakov, E., Ogilvie, S.R., Taylor, C.W., and Glover, P.W.J., 2001, Fluid flow through rough fractures in rocks I: High resolution aperture determinations: Earth and Planetary Science Letters, v. 191, p. 267–282, doi:10.1016/S0012-821X(01)00424-1.

Johns, R.A., Steude, J.S., Castanier, L.M., and Roberts, P.V., 1993, Nondestructive measurements of fracture aperture in crystalline rock cores using X ray computed tomography: Journal of Geophysical Research, v. 98, no. B2, p. 1889–1900, doi:10.1029/92JB02298.

Karpyn, Z.T., Alajmi, A., Radaelli, F., Halleck, P.M., and Grader, A.S., 2009, X-ray CT and hydraulic evidence for a relationship between fracture conductivity and adjacent matrix porosity: Engineering Geology, v. 103, p. 139–145, doi:10.1016/j.enggeo.2008.06.017.

Keller, A.A., 1997, High resolution CAT imaging of fractures in consolidated materials: International Journal of Rock Mechanics and Mining Sciences, v. 34, p. 155.e1–155.e16, doi:10.1016/S1365-1609(97)00181-0.

Ketcham, R.A., and Carlson, W.D., 2001, Acquisition, optimization and interpretation of X-ray computed tomographic imagery: Applications to the geosciences: Computers & Geosciences, v. 27, p. 381–400, doi:10.1016/S0098-3004(00)00116-3.

Ketcham, R.A., Slottke, D.T., and Sharp, J.M., Jr., 2010, Three-dimensional measurement of fractures in heterogeneous materials using high-resolution computed tomography: Geosphere, v. 6, p. 499–514, doi:10.1130/GES00552.1.

Muralidharan, V., Hakravarthy, D., Putra, E., and Schechter, D.S., 2004, Investigating fracture aperture distribution under various stress conditions using X-ray CT scanner: Canadian International Petroleum Conference, 5th, paper 2004-230, 14 p.

Pini, R., Krevor, S.C.M., and Benson, S.M., 2012, Capillary pressure and heterogeneity for the CO_2/water system in sandstone rocks at reservoir conditions: Advances in Water Resources, v. 38, p. 48–59, doi:10.1016/j.advwatres.2011.12.007.

Pyrak-Nolte, L.J., Myer, L.R., Cook, N.G., and Witherspoon, R.A., 1987, Hydraulic and mechanical properties of natural fractures in low permeability rock, Proceedings, 6th International Society of Rock Mechanics Congress: Rotterdam, A.A. Balkema, p. 225–232.

Schrauf, T.W., and Evans, D.D., 1986, Laboratory studies of gas flow through a single natural fracture: Water Resources Research, v. 22, p. 1038–1050, doi:10.1029/WR022i007p01038.

Taylor, J.R., 1997, An introduction to error analysis: The study of uncertainties in physical measurements (second edition): Sausalito, California, University Science Books, 328 p.

Vandersteen, K., Busselen, B., Van Den Abeele, K., and Carmeliet, J., 2003, Quantitative characterization of fracture apertures using microfocus computed tomography, *in* Akin, S., and Kovscek, A.R., eds., Applications of X-ray computed tomography in the geosciences: Geological Society of London Special Publication 215, p. 61–68, doi:10.1144/GSL.SP.2003.215.01.06.

Van Geet, M., and Swennen, R., 2001, Quantitative 3D-fracture analysis by means of microfocus X-ray computer tomography (μCT): an example from coal: Geophysical Research Letters, v. 28, p. 3333–3336, doi:10.1029/2001GL013247.

Weerakone, W.M.S.B., and Wong, R.C.K., 2006, Characterization of variable aperture rock fractures using X-ray computer tomography, *in* Desrues, J., et al., eds., Advances in X-ray tomography for geomaterials: London, Wiley-ISTE Ltd., p. 229–235, doi:10.1002/9780470612187.ch21.

Wolter, K., 2003, Introduction to variance estimation: New York, Springer, 431 p.